钛表面微凹凸织构的激光加工及其细胞黏附研究

何婉盈[1,2]，姚鹏[1,2*]，褚东凯[1,2]，孙惠强[3]，来庆国[4]，王庆伟[1,2]，王鹏飞[1,2]，屈硕硕[1,2]，黄传真[5]

[1]山东大学机械工程学院先进射流工程技术研究中心，山东 济南 250061；
[2]高效洁净机械制造教育部重点实验室，山东 济南 250061；
[3]山东大学口腔医学院修复科，山东省口腔组织再生重点实验室，山东 济南 250012；
[4]山东大学第二医院口腔颌面外科，山东 济南 250033；
[5]燕山大学机械工程学院，河北 秦皇岛 066004

摘要 钛以其优异的力学性能和良好的生物相容性而被广泛用于制造医疗植入体。为提高钛在人体内的稳定性、抗菌性等，需对其表面进行修饰改性。本研究采用飞秒和皮秒激光在钛表面加工出微凹槽和微凸起结构，对比了两种激光技术在钛表面加工的微凸起和微凹槽结构在表面形貌、亲疏水性和生物相容性等方面的差异。表面形貌、轮廓、元素的表征结果表明两种激光加工结构的尺寸主要受能量密度的影响，而形状受光斑重叠率的影响较大，皮秒激光加工表面的氧含量较高。由于飞秒和皮秒激光改性钛表面微织构形貌的差异，水接触角（以下简称"接触角"）从初始的 40.25° 分别降为 9.88° 和 0°。通过对比样品在空气、真空、生理盐水中保存 3 d 后的表面接触角发现，皮秒激光加工样品表面能保持稳定的超亲水性；经硅烷处理后，飞秒激光改性表面的接触角可达 152.80°，而皮秒激光改性表面的接触角为 146.38°。细胞黏附和增殖的实验结果表明飞秒激光加工的微凸起或微凹槽线阵有利于细胞的黏附和排列，而皮秒激光加工的微凸起或微凹槽线阵有利于促进细胞的铺展和迁移。

关键词 激光技术；钛；微凸起；微凹槽；润湿性；生物相容性

中图分类号 TN249　　　　**文献标志码** A　　　　　　　　　　　　　**DOI**：10.3788/CJL202249.1002605

1 引　　言

医用金属材料强度和硬度较高、韧性和加工性能良好，可以基本满足人体植入物所必需的力学性能及生物学方面的要求，已逐渐超越医用陶瓷和医用高分子材料成为植入体的首选材料[1-2]，常被用于人造关节、螺钉、骨板、髓内钉、起搏器外壳、脊柱固定器、人造心脏瓣膜、血管支架和牙种植体等[3]。与医用不锈钢及钴铬合金相比，钛及其合金密度较小、耐蚀性较好，弹性模量接近人体骨组织，可以有效降低"应力遮挡"效应[4-5]，因此成为临床应用最广泛的种植材料之一[6]。然而，钛及其合金目前仍存在一些问题，如表面生物活性不足从而导致其无法实现较好的化学性骨结合[7]，易引发宿主的炎症反应从

而导致愈合延迟[8]等。为了解决以上问题，一些学者通过改变植入体表面的显微组织形态或化学成分来增强表面的生物活性：赵梓贺等[9]利用纳秒激光结合阳极氧化，在纯钛表面制备出微沟槽-二氧化钛纳米管复合结构，该结构可以促进羟基磷灰石的沉积；Wang 等[10]结合研磨、蚀刻和阳极氧化在钛表面制备出能够诱导细胞定向分化的纳米管；Zwahr等[11]采用双光束皮秒激光干涉技术在钛表面加工出周期为 3～17 μm 的线阵，该结构能促进细胞黏附和增殖。虽然上述方法已经可以高效、高质量地对植入体表面进行加工，但其加工难以靶向进行，工艺复杂，易产生污染，且制备的表面结构质量较差，亟须开发新型高效的加工技术，以满足日益增长的植入体加工需求。

超快激光具有极高的峰值功率和极短的脉冲宽度[12]，几乎可以对任何材料进行加工[13-20]，且具有热效应小、加工精度高、三维加工能力强等独特优势，不仅可以主动控制表面加工区域，直接加工出微纳多级结构，而且能够产生表面氧化层，获得较高的表面能，进而有利于促进细胞黏附[21]。目前已有学者利用超快激光技术进行了表面纹理化：Chen 等[22]利用飞秒激光在钛表面加工微织构，结果发现微纳网格结构更能促进成骨分化；Yang 等[23]使用聚焦飞秒贝塞尔光束制造尺寸、几何形状和分布可控的微管（SZ2080 光刻胶）阵列，并通过单细胞操作证明该微管可以参与微粒和细胞的准确捕获、转移和释放；Yong 等[24]采用飞秒激光在聚对苯二甲酸乙二醇酯（PET）表面制备多孔网络结构，并结合化学处理获得光滑表面，该表面可以完全抑制神经胶质瘤细胞（C6）的生长。虽然上述研究说明飞秒激光已经可以制备特定功能的表面，但其加工的结构类型较少，工艺较复杂，且加工效率较低，亟须调整和优化工艺，提高钛表面微织构的多样性及加工效率。

本研究团队首先通过改变飞秒激光和皮秒激光工艺参数，在钛表面直写出微凹槽和微凸起结构；之后系统研究了飞秒激光和皮秒激光制备钛表面微织构的差异，讨论了激光改性前后样品表面浸润性的变化，探索了浸润性调控的后处理方法；最后基于细胞黏附和增殖实验对不同微织构表面的生物学性能进行评价。本研究为钛植入体表面改性提供了新方法，扩展了钛表面微织构的类型，为钛植入体应用领域的拓展提供了参考。

2 材料和方法

2.1 样品预处理

采用线切割将厚度为 1 mm 的纯钛板切成直径为 10 mm 的钛圆片，然后依次采用 250♯、600♯、800♯、2000♯ 砂纸对钛圆片进行打磨，去除其表面的氧化层，再用金刚石抛光剂配合红丝绒将其抛光至表面无划痕。将抛光后的试件放入无水乙醇中超声清洗 10 min，重复 2 次，以去除表面污染物，随后自然晾干。

2.2 激光加工与后处理

采用飞秒激光（Spectra Physics Spitfire Ace 钛蓝宝石激光系统，脉宽 W 为 35 fs，波长 λ 为 800 nm，重复频率 P_{RF} 为 1 kHz，峰值功率 12 W）和皮秒激光（天津凯普林光电科技有限公司 BGL-

1064-50B 激光器，脉宽 W 为 15 ps，波长 λ 为 1064 nm，重复频率 P_{RF} 为 10～1000 kHz，最大扫描速度为 5 m/s，最大功率为 50 W）对钛表面进行改性加工。将改性后的样品分别进行自然放置、生理盐水（0.9% NaCl）浸泡、真空密封保存，对比这三种后处理工艺对样品亲水稳定性的影响。将样品置于 1H,1H,2H,2H-全氟癸基三乙氧基硅烷溶液[分子式为 $C_{16}H_{19}O_3F_{17}Si$，乙醇稀释为 1%（体积分数）]中浸泡 1 d[25]后自然晾干，以降低样品的表面能。

2.3 细胞黏附和增殖

样品经高温高压消毒后，放入 24 孔板，每孔接种大鼠骨髓间充质干细胞（rBMSCs）$4×10^4$ 个（1∶4 传代），然后置于 37 ℃ 二氧化碳培养箱中培养 48 h；取出样品，用缓冲液（PBS）轻轻洗去未黏附的细胞；室温下，将样品浸泡在 4% 多聚甲醛溶液中 1 h，以固定细胞；使用体积分数为 20%、30%、40%、50%、60%、70%、80%、90%、100% 的乙醇溶液梯度脱水，每种浓度下脱水 10 min；自然晾干后喷金固定，观察表面的细胞黏附情况。

将消毒后的样品放入 24 孔板，每孔接种细胞 $5×10^4$ 个，分别在培养 1,3,5 d 时吸取细胞悬浮液 100 μL，接种到新的 24 孔板中，每孔加入 10 μL CCK-8 溶液，培养 0.5 h 后，用酶标仪测定各孔细胞悬浮液在 450 nm 处的吸光度。

2.4 表面表征

使用 JSM-6610LV 型扫描电子显微镜（SEM）观察样品的表面形貌，采用 VK-X200 型激光共聚焦显微镜（CLSM）表征样品的表面轮廓，采用 JSM-6610LV 能量色散 X 射线光谱仪（EDS）分析样品表面的元素种类及含量，采用 SDC-200S 型静态接触角测量仪测量样品表面的水接触角（以下简称"接触角"），使用 M200 PRO NanoQuant 酶标仪测量细胞悬浮液的吸光度。

3 分析与讨论

3.1 微织构形成机理分析

材料烧蚀阈值与入射激光的脉宽息息相关，并对表面形貌有重要影响。本研究采用飞秒激光（脉冲个数为 100，入射能量 E 分别为 1.13，3.19，5.24，7.29，9.34，11.40，13.45，15.50，17.56，19.61 μJ）和皮秒激光（脉冲个数为 100，入射能量 E 分别为 258.05，310.92，361.62，415.52，468.27，517.80 μJ）多脉冲烧蚀钛表面，多次测量烧蚀孔直径 D 并求出平均值，通过数值计算法建立烧蚀孔直

径 D 与入射能量 E 之间的数学关系,计算出束腰半径 ω_0 和多脉冲烧蚀阈值[26],再通过脉冲个数与烧蚀阈值间的数学关系计算获得单脉冲烧蚀阈值 φ_{th}[27],最终求得飞秒激光光束的束腰半径 ω_0 为 14.53 μm,其加工钛的单脉冲烧蚀阈值 φ_{th} 为 1.01 J/cm²,皮秒激光光束的束腰半径 ω_0 为 59.67 μm,其加工钛的单脉冲烧蚀阈值 φ_{th} 为 3.23 J/cm²。测量及计算结果如表 1 所示。

表 1　不同脉宽激光入射时钛的烧蚀阈值

Table 1　Ablation threshold of titanium under laser with different pulse widths

Laser	W /fs	P_{RF}/kHz	λ /nm	E /μJ	D /μm	ω_0/μm	φ_{th}/(J·cm^{-2})
Femtosecond laser	35	1	800	1.13, 3.19, 5.24, 7.29, 9.34, 11.40, 13.45, 15.50, 17.56, 19.61	7.38, 15.44, 20.11, 22.89, 25.47, 27.47, 30.27, 31.60, 34.40, 35.20	14.53	1.01
Picosecond laser	15	100	1064	258.05, 310.92, 361.62, 415.52, 468.27, 517.80	92.00, 95.00, 99.00, 110.00, 115.76, 110.69	59.67	3.23

飞秒激光加工金属表面的作用机理可以概括为:金属表面电子吸收光子后被激发,形成热电子,热电子与冷晶格之间建立热平衡;当晶格温度升高到足够高时,发生熔化和烧蚀,烧蚀中的等离子体羽流由中性原子、离子、团簇和纳米粒子组成;烧蚀之后,表面以极高的速率冷却,并迅速凝固,生成表面结构。研究发现,当激光参数选取合适时,采用飞秒激光在钛表面不仅可以制备出传统的微凹槽结构,还可以制备出微凸起结构。不同微织构的形成机理可以通过激光的光热作用和马兰戈尼对流作用[28]来解释。当激光聚焦到样品表面,且表面晶格温度升到足够高时,表面熔化结合羽流向外对流形成传统的微凹槽结构,重铸层往往较多。本研究在光斑重叠率较低时离焦加工,使高能量处的羽流快速扩散,同时对流作用将热传递到钛表面,使其熔化形成重铸层较少的凹槽结构;同时在光斑重叠率较高时离焦加工,使钛表面产生的等离子体羽流在高能位置处反复熔化,对流作用将微粒、团簇等向下传递,最终在急速冷却后重新凝固形成凸起结构。图 1 所示为不同飞秒激光工艺参数下钛表面微织构形貌的演变规律。当光斑直径为 29.06 μm、能量密度为 3.90 J/cm² 时,通过增大扫描速度使光斑重叠率降低(从 97.94% 逐渐降低到 96.56%),结果发现边缘重铸层减少,热影响区变窄,激光诱导周期性条纹[29](LIPSS)的连续性降低,如图 1(a2)~(a4)所示。这是由于随着光斑重叠率降低,有效脉冲数减少,积累的能量减少,等离子体羽流中的微粒在弱对流作用下向两边扩散并且快速凝固,从而形成带有明显重铸层的凹槽结构,同时边缘区域激光散射波与入射波的相互干涉作用[30]减弱,LIPSS 的连续性下降。当光斑直径和能量密度不变、光斑重叠率为 96.56% 时加工出的凹槽呈 V 形,如图 1(b2)所示,

这是由于激光能量呈高斯分布[31]。随离焦量增加,激光光斑直径逐渐增大,能量密度逐渐减小,激光烧蚀区域内的能量差异减小,表面烧蚀更加均匀,凹槽形状逐渐接近 U 型,如图 1(b3)~(b4)所示;同时,由于到达槽底的能量密度接近烧蚀阈值,因此槽底形成了较多微米颗粒,边缘重铸层减少,热影响区减小。随着能量密度增大,边缘重铸层明显增多,热影响区扩大,且出现了较多条状微粒,如图 1(c2)~(c4)所示。

与凹槽结构相比,凸起结构主要在光斑重叠率较高时形成。这是由于此时的有效脉冲数较多,单位面积内的激光能量高,对流作用较强,使得微粒来不及向边缘扩散便快速重新凝固在凹槽上方,从而形成空心的凸起结构。通过增大扫描速度可以使光斑重叠率降低,此时有效脉冲数逐渐减少,对流时间变短,凸起的组成颗粒变大,表面孔隙减少,热影响区宽度减小,同时边缘的波纹槽[32]由于能量辐射减弱而逐渐减少,如图 1(d2)~(d4)所示。随着离焦量增加,光斑直径变大,激光能量密度降低,对流作用减弱,同时由于超快激光加工过程中微粒凝固速度较快,因此微粒不均匀成簇,如图 1(e2)~(e4)所示;与此同时,热影响减弱,边缘重铸层和波纹槽减少。随着能量密度增大,羽流中的微粒较多且对流剧烈,颗粒堆积得更加致密,热影响区扩大,边缘重铸层和波纹槽均增多,如图 1(f2)~(f4)所示。

不仅飞秒激光可以在适当的工艺参数下制备出微凹槽和微凸起结构,皮秒激光以其功率大、脉宽短的特性也能在钛表面加工出微凹槽和微凸起结构。图 2 所示为不同皮秒激光加工参数下钛表面微织构形貌的演变规律。当光斑直径为 119.34 μm、光斑重叠率为 97.32% 时,随着能量密度增加,激光烧蚀作用增强,表面结构从平面微孔变为底部褶皱逐渐增
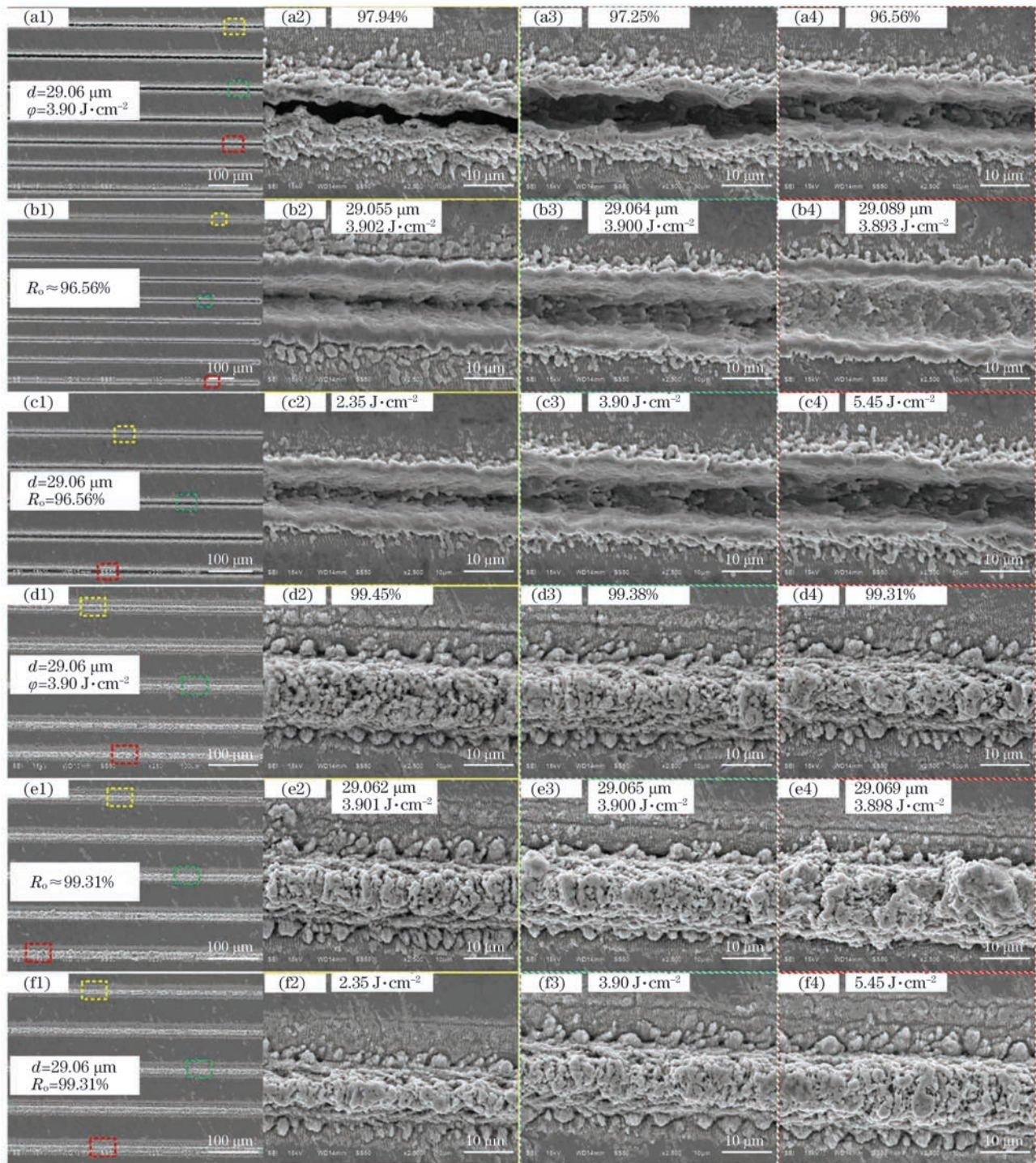
图 1 飞秒激光加工微凹槽(a)～(c)和微凸起(d)～(f)的 SEM 图。(a)(d)变光斑重叠率;(b)(e)变光斑直径、能量密度和光斑重叠率;(c)(f)变能量密度

Fig. 1 SEM images of femtosecond laser processed microgroove (a)−(c) and microprotrusion (d)−(f). (a)(d) Different overlapping rates (R_O); (b)(e) different spot diameters (d), laser influences (φ), and overlapping rates; (c)(f) different laser influences

多的凹槽,边缘重铸层也明显增加,如图 2(a1)～(a5)所示。当能量密度为 5.54 J/cm² 时,通过增加扫描速度使光斑重叠率逐渐降低,结果发现单位面积烧蚀作用减弱,凹槽底部褶皱和边缘重铸层均减少,如

图 2(b1)～(b5)所示。通过增大重复频率使光斑重叠率由 73.19% 逐渐提高至 97.32% 时,表面形貌由波纹状分布的微孔变为连续分布的微孔,并最终形成底部有褶皱的凹槽,如图 2(c1)～(c4)所示。这是由

于光斑边缘区域的能量密度逐渐增加,甚至超过烧蚀阈值,形成明显的材料去除,而当光斑重叠率较高(如重叠率为 98.66%)时,重铸层明显向内积聚,如图 2(c5)所示。这是由于此时的有效脉冲数较多,表面对流作用增强。当光斑重叠率为 99.16% 时,随着能量密度增大,重铸层继续向内积聚,形成凸起结构,如图 2(d1)~(d2)所示。当能量密度为 3.24 J/cm^2 时,随着光斑重叠率逐渐降低,凸起结构顶部逐渐出

现裂缝,如图 2(e1)~(e2)所示。这是因为此时的有效脉冲数减少,对流作用减弱。当光斑重叠率为 99.67% 时,随着能量密度由 5.54 J/cm^2 逐渐增至 9.26 J/cm^2,钛表面出现组成颗粒较大的凸起结构,边缘密布微米颗粒,如图 2(f1)~(f2)所示。这主要是因为此时有效脉冲数较多且能量密度较高,对流增强,导致微粒熔融后聚集,并快速凝固成大颗粒;与此同时,随着能量密度增大,颗粒长大且排列得更紧密。
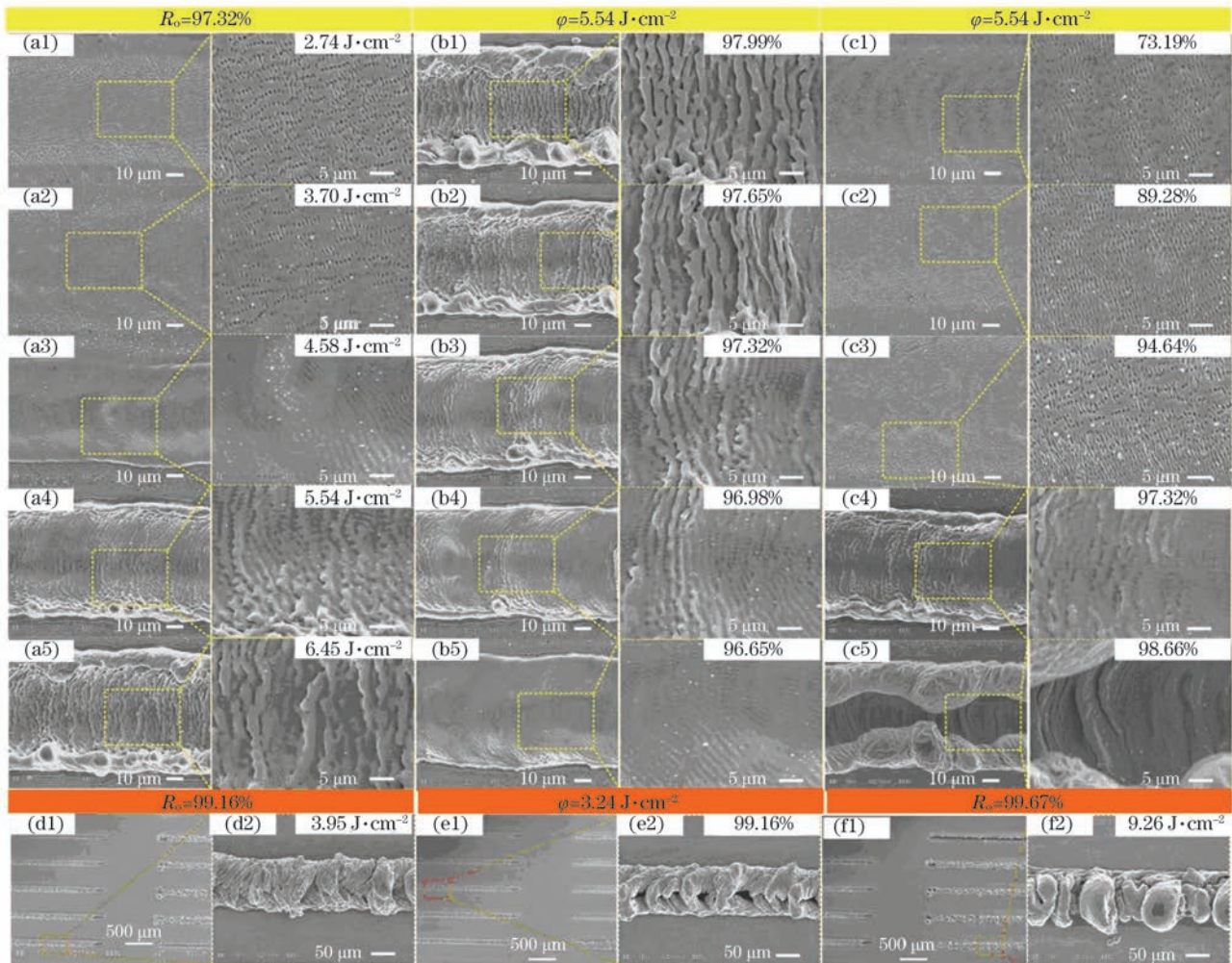

图 2 皮秒激光加工微凹槽(a)~(c)和微凸起(d)~(f)的 SEM 图。(a)(d)(f)变能量密度;(b)(c)(e)变光斑重叠率

Fig. 2 SEM images of picosecond laser processed microgroove (a)–(c) and microprotrusion (d)–(f).
(a)(d)(f) Different laser influences (φ); (b)(c)(e) different overlapping rates (R_O)

3.2 微织构表面润湿性能表征及其机理研究

基于仿生学的发展,亲/疏水表面在自清洁[33]、油水分离[34]、防冰抗冻[35]、水面减阻[36] 等方面的应用越来越广泛。同时,由于材料的表面能、润湿性、表面电荷、表面化学成分和表面形貌等对细胞或细菌在表面的黏附有影响或共同影响[37-40],因此,亲疏水功能表面的制备方法在植入体改性中也具有潜在的应用价值。材料表面的亲疏水性能主要受表面微

织构形貌及化学元素的影响。

图 3 所示为飞秒激光加工参数变化时表面微凹槽和微凸起轮廓的测量结果。当光斑直径为 29.06 μm、能量密度为 3.90 J/cm^2、光斑重叠率为 97.94% 时,有效脉冲数较多,导致重铸层较厚,掩盖了底部的凹槽,表面轮廓接近凸起结构,如图 1(a2) 所示;随着有效脉冲数的减少,槽深减小,重铸层减少,如图 3(a)所示。随着离焦量增加,激光光斑直

径逐渐增加,导致槽宽逐渐增大,同时能量密度逐渐降低,导致深度逐渐减小,如图 3(b)所示。通过增大功率使能量密度增大时,槽宽和槽深均小幅度增加,边缘重铸层逐渐变高,如图 3(c)所示。在以上加工参数变化过程中,由于到达底部的激光能量逐渐均匀,凹槽均趋近 U 形,且这种现象在光斑直径增大或光斑重叠率降低时较为明显。对于凸起结构,随着光斑重叠率降低,有效脉冲数减少,结构宽度减小,高度增加,顶部逐渐尖锐。这是因为此时的对流时间缩短,羽流中的部分微粒来不及向下传递

而在顶部累积,最终导致凸起顶部近似倒 V 形,如图 3(d)所示。当有效脉冲数较多时,随着光斑直径小幅度增大,凸起宽度、高度均增加,如图 3(e)所示;而随着能量密度大幅度增大,凸起宽度、高度均显著增加,且凸起顶部趋向平整,如图 3(f)所示。总的来说,在飞秒激光工艺参数中,由离焦量变化引起的光斑直径和能量密度变化对结构的宽度和深(高)度影响较大,由功率改变引起的能量密度变化的影响次之,由改变速度引起的光斑重叠率变化的影响最小(但其对凹槽底部和凸起顶部平整度的影响较大)。
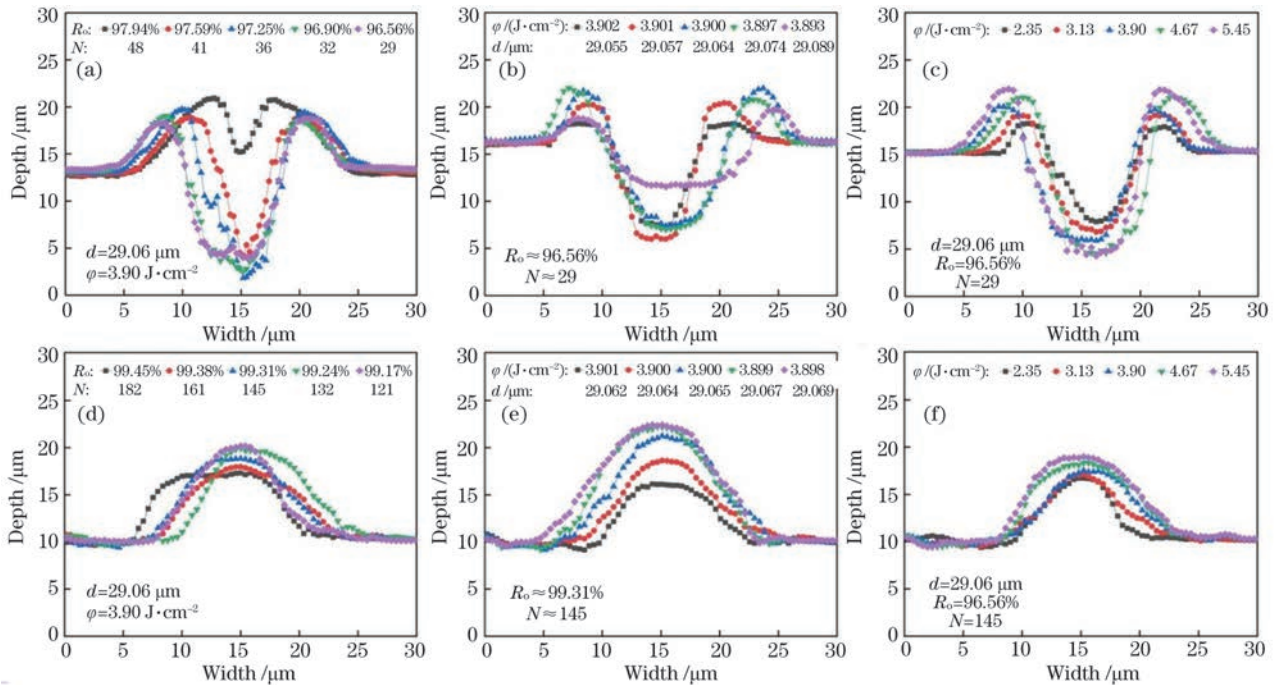

图 3　飞秒激光加工微凹槽(a)～(c)和微凸起(d)～(f)的表面轮廓。(a)(d)变光斑重叠率(有效脉冲数);(b)(e)变光斑直径、能量密度和光斑重叠率(有效脉冲数);(c)(f)变能量密度

Fig. 3　Surface profiles of femtosecond laser processed microgroove (a)−(c) and microprotrusion (d)−(f). (a)(d) Different overlapping rates〔pulse number (N)〕; (b)(e) different spot diameters, laser influences and overlapping rates (pulse number); (c)(f) different laser influences

　　图 4 所示为皮秒激光加工参数变化时表面微凹槽和微凸起的轮廓测量结果。当能量密度或光斑重叠率较低时,钛表面烧蚀效果不明显,如图 4(a)、(c)所示。随着能量密度增大,凹槽宽度不变,深度增加,边缘重铸层增高,如图 4(a)所示。增大扫描速度使光斑重叠率降低,有效脉冲数减少,此时槽宽增大,槽深减小,重铸层降低,如图 4(b)所示。增大重复频率使光斑重叠率提高,有效脉冲数增多,此时重铸层增多,并逐渐向内积聚,接近凸起结构,如图 4(c)所示。对于微凸起结构,当能量密度增大或光斑重叠率增大时,凸起的宽度和高度均逐渐增大,如图 4(d)～(e)所示。当光斑重叠率为 99.67% 时,随着能量密度在较大范围内逐渐增大,大颗粒凸起

的宽度和高度明显增大,如图 4(f)所示。总的来说,皮秒激光加工结构的尺寸受能量密度的影响较大,形状受光斑重叠率的影响较大,微凸起不仅尺寸远大于微凹槽,而且只形成于光斑重叠率较高时。

　　飞秒激光烧蚀金属表面时常发生剧烈的氧化反应,表面生成金属氧化物,同时表面自由能得到提高。图 5 所示为飞秒和皮秒激光加工线阵的表面形貌和 EDS 表征结果。对于飞秒激光加工的线阵,根据其表面形貌可将凹槽分为两组:一组的重铸层向内积聚,如图 5(a3)所示,将其命名为"凹槽 1 组";另一组的重铸层向外堆积,如图 5(a4)所示,将其命名为"凹槽 2 组"。分析元素含量可以发现,飞秒微织构表面的氧含量均增加,其中图 5(a2)所示的凸
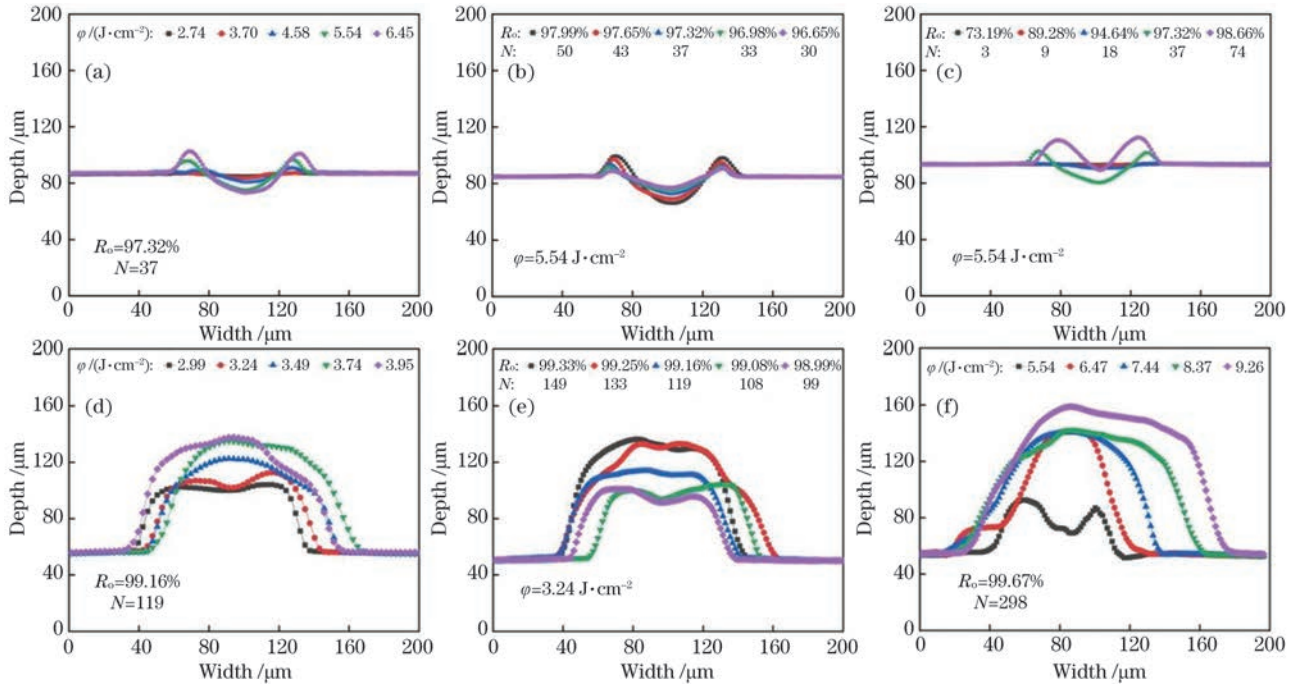
图 4 皮秒激光加工微凹槽(a)～(c)和微凸起(d)～(f)的表面轮廓。(a)(d)(f)变能量密度;(b)(c)(e)变光斑重叠率(有效脉冲数)

Fig. 4 Surface profile of picosecond laser processed microgroove (a)−(c) and microprotrusion (d)−(f).
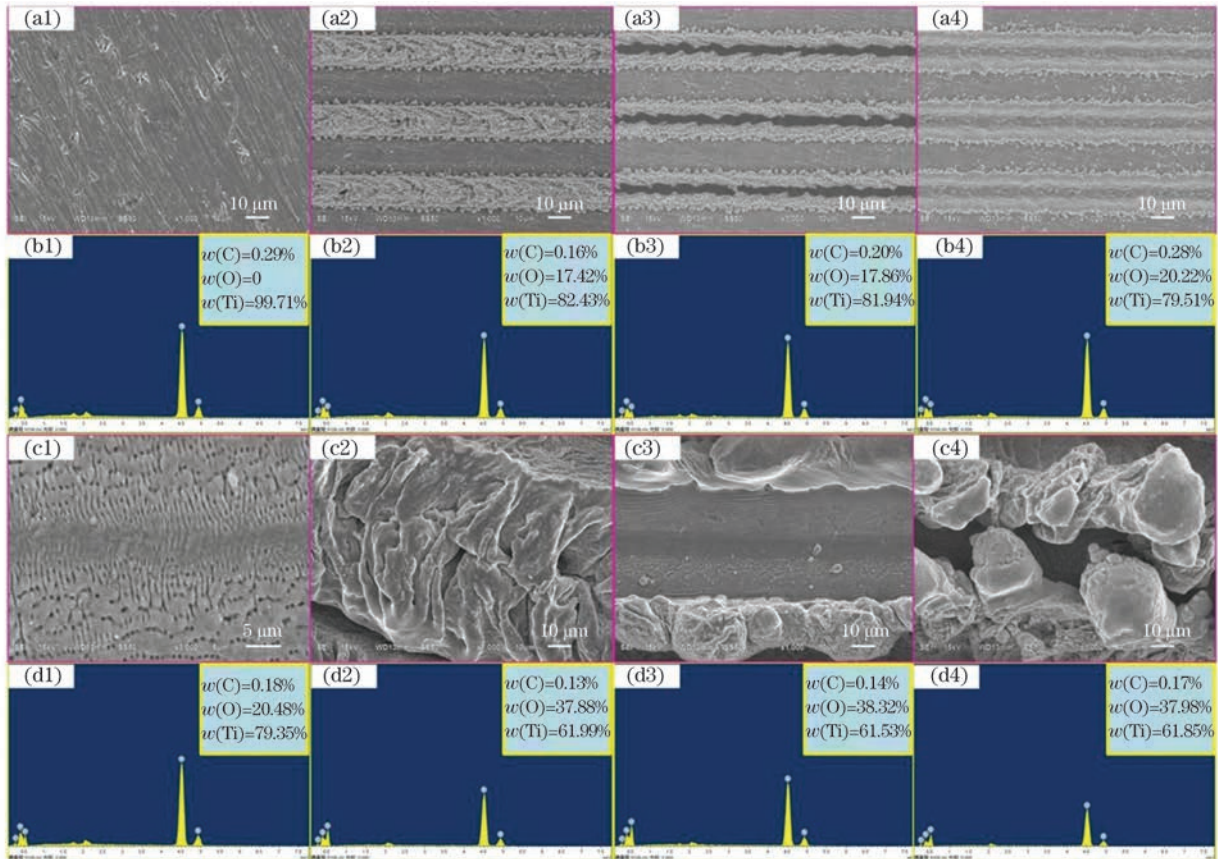(a)(d)(f) Different laser influences; (b)(c)(e) different overlapping rates (pulse number)

图 5 不同激光加工线阵的 SEM 图和 EDS 结果。(a)(b)飞秒激光加工;(c)(d)皮秒激光加工

Fig. 5 SEM images and EDS results of laser processed liner array. (a)(b) Femtosecond laser processing;
(c)(d) picosecond laser processing

起组的氧含量与凹槽 1 组接近,但都低于凹槽 2 组。这是因为凹槽 2 组的烧蚀面积较大,因此表面氧含量可达 20.22%(质量分数),如图 5(b2)～(b4)所示。对于皮秒激光加工的线阵,根据其表面形貌的差异也可将凹槽分为两组:一组的重铸层向内收缩,且较为连续,如图 5(c3)所示,将其命名为"凹槽 1 组";另一组的重铸层向外展开,分布不连续,形成的颗粒较大,如图 5(c4)所示,将其命名为"凹槽 2 组"。由于皮秒激光的单脉冲能量和脉宽均比飞秒激光大,因此烧蚀作用更加剧烈,表面氧含量明显增多,如图 5(d1)～(d4)所示,其中皮秒激光加工的微孔组[如图 5(c1)所示]由于能量密度和光斑重叠率均较低,表面氧含量相对较低,而凸起组[如图 5(c2)所示]、凹槽 1 组、凹槽 2 组是在较高的能量密度作用下形成的,表面氧含量可达 38.32%(质量分数),约为微孔组的 2 倍。

图 6 所示为不同激光加工间距下的表面接触角测量结果。飞秒激光改性后,钛表面接触角由最初的 40.25° 减至最小 9.88°,亲水性变好。其改性机理是激光烧蚀钛表面会生成较多氧化物(Ti_xO_y),表面氧空穴易被空气中的水分子取代形成羟基(—OH),羟基较多时,表面会更加亲水[41]。当激光加工间距较小时,凸起线阵的亲水性比凹槽线阵好。这是因为凸起结构顶部富含氧化物,能加快水滴在表面的铺展,此时两种结构均遵循 Wenzel 模型[42],表面接触角随间距的减小而减小。当加工间距较大时,凹槽与凸起线阵表面接触角的差异减小,如图 6(a)所示。这是由于此时加工间距远大于结构宽度,表面粗糙度差异变小。

不同后处理工艺会使飞秒激光改性样品表面润湿性发生较大改变。当样品在空气中自然放置时,其表面能较高,容易通过自发吸附空气中的低表面能有机物(C_mH_n)来降低自身的表面能[43],此时表面的亲水性变差,甚至变为疏水表面。通过对比图 6(b)～(c)所示的在空气、真空、生理盐水中分别保存 3 d 的样品表面的接触角可以发现,飞秒激光改性样品在空气中自然放置时,表面亲水性均变差,而当在真空和生理盐水中保存 3 d 后,由于表面隔
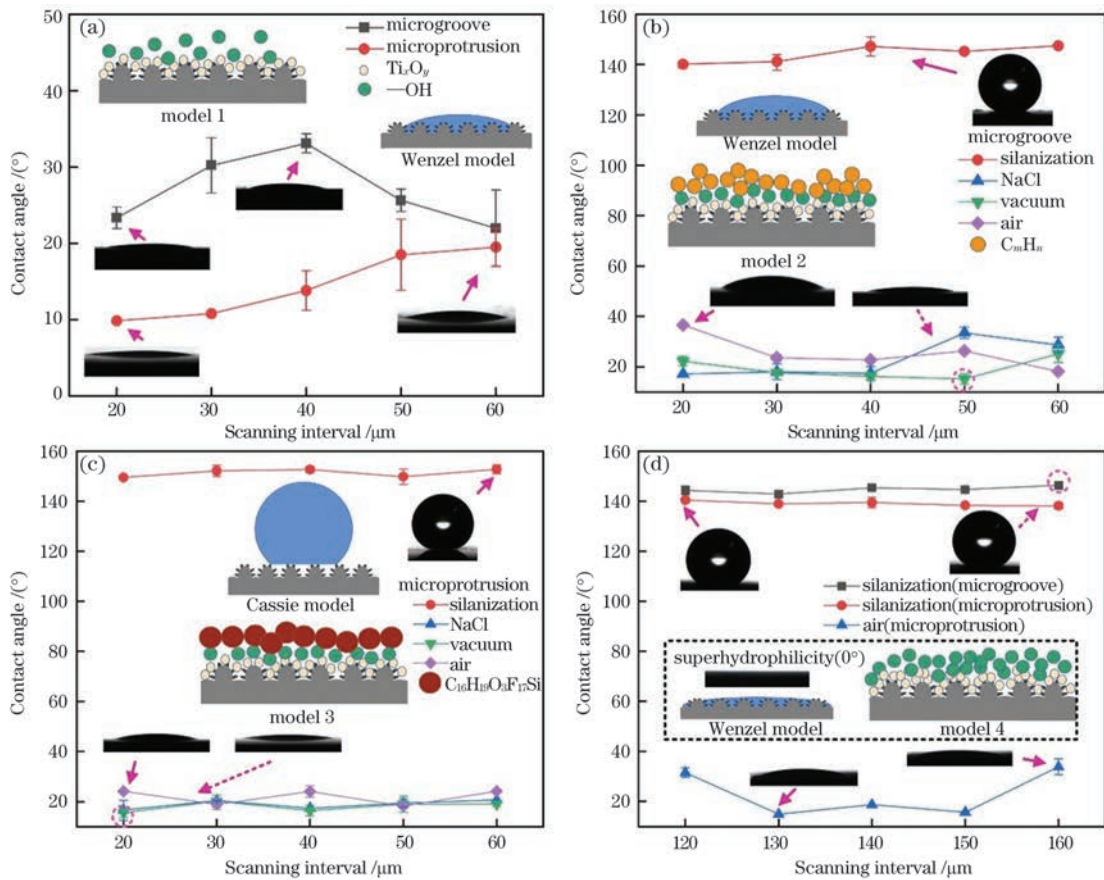

图 6　不同间距线阵表面的接触角。(a)飞秒激光加工表面;(b)(c)飞秒激光加工及后处理表面;(d)皮秒激光加工及后处理表面

Fig. 6　Contact angle of liner array varying with scanning interval. (a) Femtosecond laser processed surface; (b)(c) femtosecond laser processed and post-processed surface; (d) picosecond laser processed and post-processed surface

绝了有机物污染,间距较小的凹槽线阵和凸起线阵表面均能保持较好的亲水性。

样品表面经过硅烷化处理后可以获得疏水性,其机理是硅烷分子($C_{16}H_{19}O_3F_{17}Si$)会与金属表面的羟基发生脱水缩合反应而自组装在材料表面,从而获得疏水效果[44]。若同时提高表面粗糙度,疏水效果会进一步增大[45-46]。本研究发现,未经激光改性的表面通过硅烷处理后,接触角为113.63°,而飞秒激光改性并经硅烷处理的表面变为超疏水表面,接触角可达 152.80°,遵循 Cassie模型[47],如图 6(c)所示,其中凸起线阵的表面接触角较凹槽线阵略高。由此可见,飞秒激光加工能够增大表面粗糙度和固-液接触面积,进而增强表面的疏水性。

当水滴落在皮秒激光制备的凹槽或凸起线阵表面时,均能立即铺展开,达到超亲水性。这是因为与飞秒激光改性表面相比,皮秒激光改性表面的氧化程度更高,表面羟基含量增多,如图 6(d)中的虚线框所示。在真空、生理盐水后处理条件下,样品表面的超亲水性能够保持稳定。经硅烷处理后,皮秒激光表面接近超疏水,接触角最大可达 146.38°。

3.3 细胞黏附和增殖分析

植入体表面微纳米复合形貌比单纯的微米或纳米形貌更有利于成骨细胞的生物学行为,其主要机理是:微米结构可以增加植入体的表面积,增强植入体与骨细胞的机械嵌合,提高植入体的力学性能;纳米结构可以通过调节细胞间的信息传递调节其行为。飞秒激光加工技术正因为可以获得微纳双级结构而在植入体表面修饰改性领域具有较好的应用前景。图 7 所示为不同飞秒激光加工线阵表面的大鼠骨髓间充质干细胞(rBMSCs)黏附情况。对比可以发现:空白组细胞分布无规律,形态呈梭形、多边形等,如图 7(a)所示;凸起组细胞多沿顶部和边缘条纹区铺展,呈短条状,如图 7(b)所示;凹槽 1 组细胞多覆盖在重铸层及条纹区,甚至出现跨槽铺展的现象,形态较宽,连片生长,如图 7(c)所示;凹槽 2 组
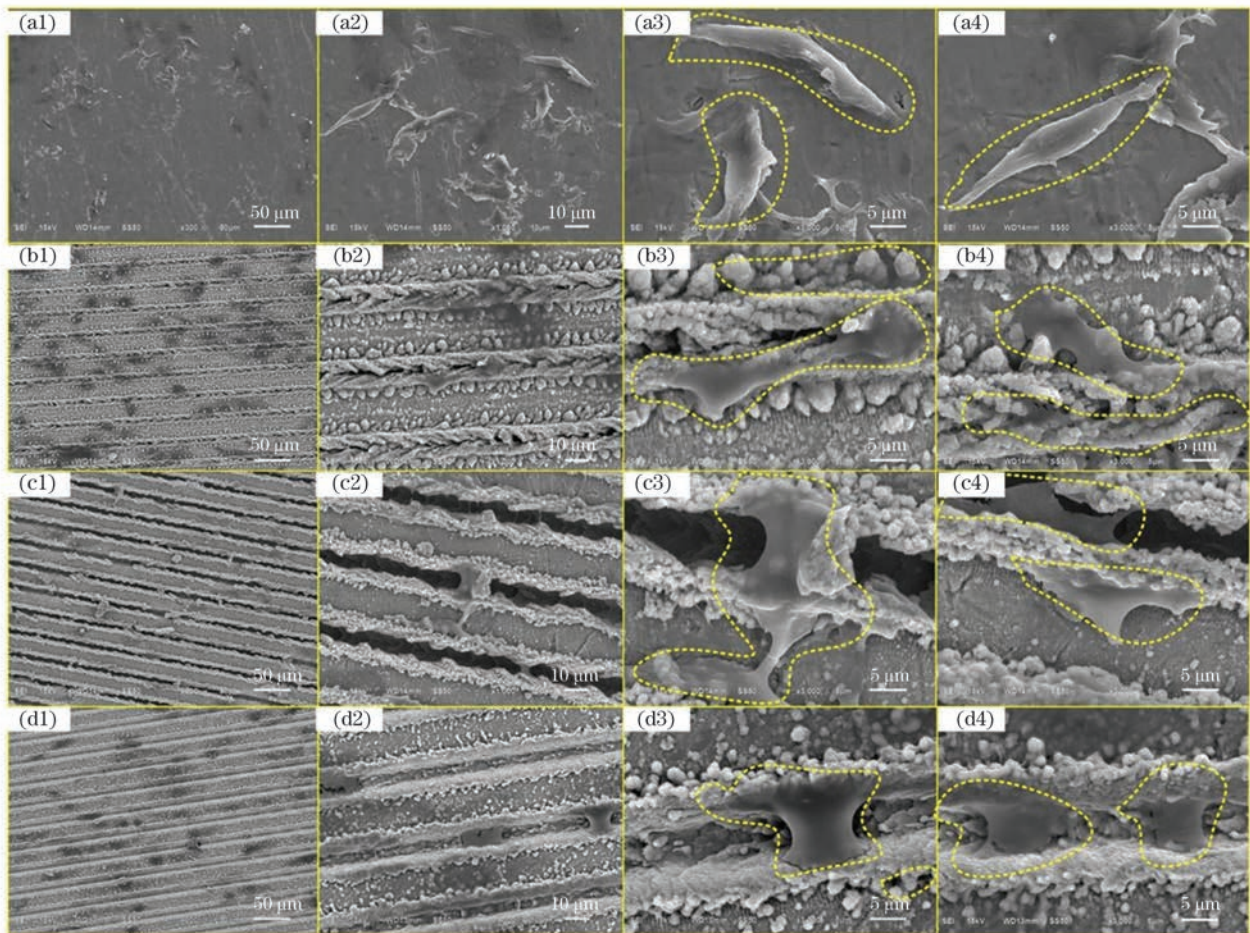

图 7 rBMSCs 在飞秒激光加工表面黏附的 SEM 图(48 h)。(a)空白组;(b)凸起组;(c)凹槽 1 组;(d)凹槽 2 组

Fig. 7 SEM images of rBMSCs adhesion on femtosecond laser processed surfaces (48 h). (a) Control; (b) microprotrusion; (c) microgroove 1; (d) microgroove 2

细胞多生长在槽内,呈薄片状,如图 7(d)所示。由此可见,飞秒激光在钛表面加工的微凸起或微凹槽线阵均会影响细胞形态,其中凸起组和凹槽 2 组的微织构更有利于细胞黏附和排列。图 8 所示为飞秒激光线阵表面的细胞增殖情况。培养 5 d 后,凸起组和凹槽2组的细胞数量显著多于凹槽1组,这与
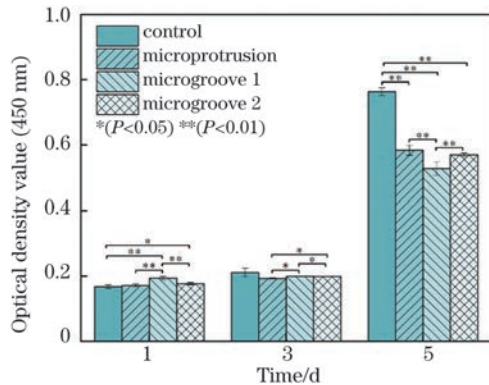
细胞黏附结果一致,如图 7(a1)～(d1)所示;同时发现线阵表面细胞数量均略少于对照组,这是由于结构在影响细胞形态和排列的同时,可能会促进部分细胞较早地成骨分化,导致增殖减少。

图 9 所示为不同皮秒激光加工线阵表面的细胞黏附情况。图 9(a)所示微孔组的细胞数量较多,且细胞分布无规律,呈多边形、梭形,能够连接成片,与图 7(a)所示的空白组相比,细胞表面积较大,有利于细胞的生命活动。凸起组细胞主要铺展在顶部褶皱内、相邻结构间隙间,且生出了较多伪足,如图 9(b)所示,有利于细胞黏附与迁移[48]。凹槽 1 组的细胞主要生长在重铸层和边缘条纹区,形态较宽,铺展良好,少数细胞沿顶部跨槽生长,如图 9(c)所示。凹槽 2 组细胞多生长在重铸层的间隔处或表面褶皱中,铺展性较差,如图 9(d)所示。总的来说,尽管皮秒激光加工表面黏附的细胞数量相对飞秒激光加工表面较少,但凸起组和凹槽 1 组能显著促进伪足生长,有利于细胞的铺展和迁移。

图 8 飞秒激光加工表面的细胞增殖情况

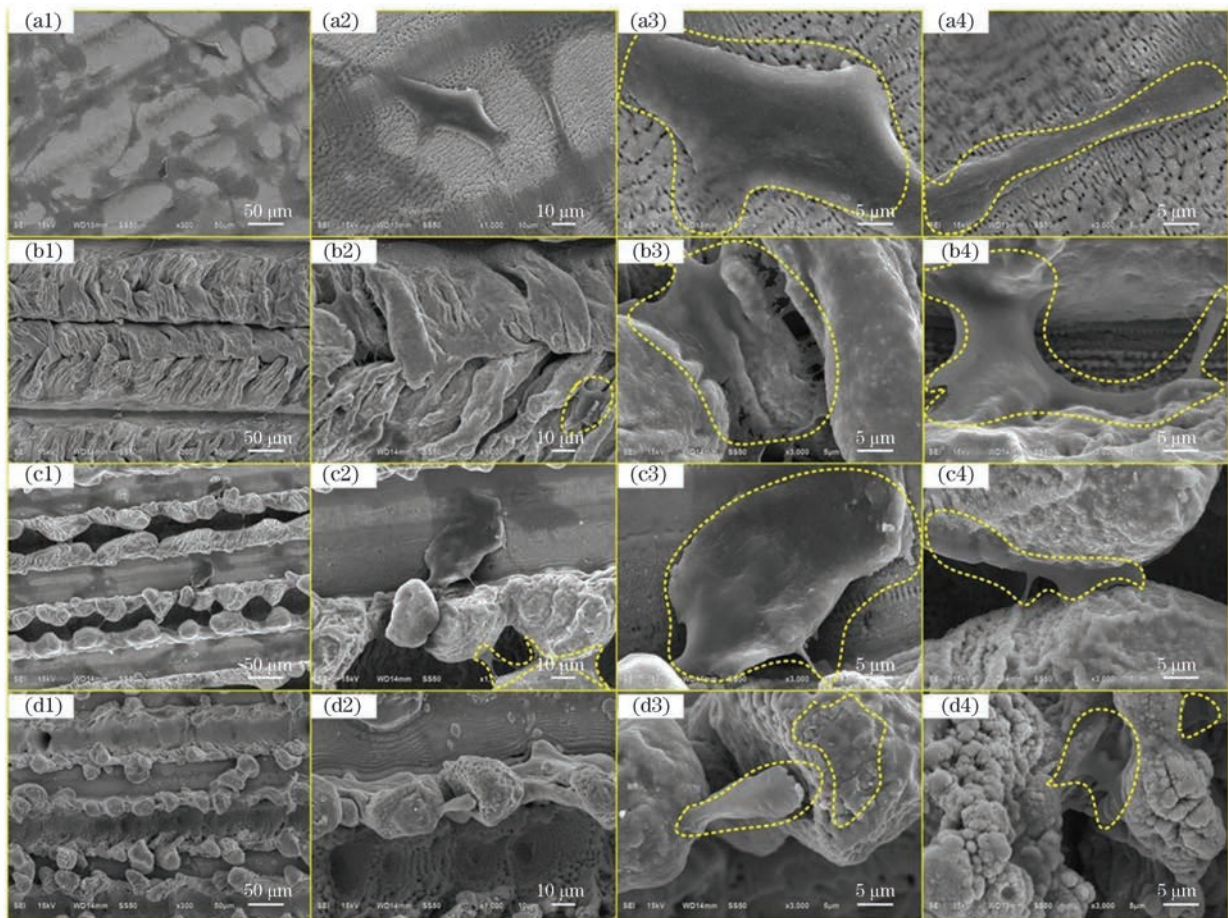Fig. 8 Cell proliferation of femtosecond laser processed surfaces

图 9 rBMSCs 在皮秒激光加工表面黏附的 SEM 图(48 h)。(a)微孔组;(b)凸起组;(c)凹槽 1 组;(d)凹槽 2 组

Fig. 9 SEM images of rBMSCs adhesion on picosecond laser processed surfaces (48 h). (a) Micropores; (b) microprotrusion; (c) microgroove 1; (d) microgroove 2

4　结　　论

本研究采用飞秒和皮秒激光在钛表面制备出微凸起和微凹槽结构,研究了不同激光参数下表面微织构的形成机理,基于微织构的表面形貌、表面轮廓、表面化学成分变化规律分析了两种激光改性表面初始亲水性的差异,探索了不同后处理工艺下表面润湿性的变化,研究了不同线阵结构对细胞黏附和增殖的影响。得出的主要结论如下:

1)飞秒激光烧蚀钛表面形成微凸起和微凹槽时,表面微粒和孔隙较多,表面氧含量可达 20.22%(质量分数),而皮秒加工表面由于烧蚀能量高,易形成褶皱,表面氧含量高达 38.32%(质量分数)。两种激光烧蚀而成的微织构的尺寸和形状分别受能量密度和光斑重叠率的影响较大,其中皮秒激光由于光斑直径较大,加工结构的尺寸远大于飞秒激光加工结构的尺寸。

2)不同激光改性表面的微织构形貌差异较大,从而影响了它们的润湿性。飞秒激光烧蚀后的钛表面接触角从初始的 40.25° 降为 9.88°,而皮秒激光加工表面可达 0°。当样品在真空、生理盐水中保存 3 d 后,皮秒激光改性表面保持稳定的超亲水性。结合硅烷处理,飞秒激光改性表面变为超疏水表面,接触角可达 152.80°,而皮秒激光制备表面的接触角为 146.38°。

3)飞秒和皮秒激光改性表面均会影响细胞的黏附效果。飞秒激光加工的微凸起或微凹槽线阵表面有利于细胞的黏附和排列,且可能促进细胞较早分化,而皮秒激光制备的微凸起或微凹槽表面有利于细胞伪足的生长,进而促进细胞的铺展和迁移。

未来更多的生物实验有待开展,以证明激光修饰改性植入体表面优异的生物相容性。超快激光微纳加工与亲/疏水表面制备工艺相结合的方法有望在增强植入体表面活性方面发挥重要作用,其中皮秒激光由于加工速度快和焦深大而在复杂形状植入体表面改性领域具有广阔的应用前景。

参 考 文 献

[1] Reznikov N, Shahar R, Weiner S. Bone hierarchical structure in three dimensions[J]. Acta Biomaterialia, 2014, 10(9): 3815-3826.

[2] Niinomi M, Nakai M, Hieda J. Development of new metallic alloys for biomedical applications[J]. Acta Biomaterialia, 2012, 8(11): 3888-3903.

[3] Kulkarni M, Mazare A, Gongadze E, et al. Titanium nanostructures for biomedical applications[J]. Nanotechnology, 2015, 26(6): 062002.

[4] Asgharzadeh Shirazi H, Ayatollahi M R, Asnafi A. To reduce the maximum stress and the stress shielding effect around a dental implant-bone interface using radial functionally graded biomaterials[J]. Computer Methods in Biomechanics and Biomedical Engineering, 2017, 20(7): 750-759.

[5] Nappi F, Carotenuto A R, di Vito D, et al. Stress-shielding, growth and remodeling of pulmonary artery reinforced with copolymer scaffold and transposed into aortic position[J]. Biomechanics and Modeling in Mechanobiology, 2016, 15(5): 1141-1157.

[6] John A A, Jaganathan S K, Supriyanto E, et al. Surface modification of titanium and its alloys for the enhancement of osseointegration in orthopaedics[J]. Current Science, 2016, 111(6): 1003-1015.

[7] Kokovic V, Jung R, Feloutzis A, et al. Immediate vs. early loading of SLA implants in the posterior mandible: 5-year results of randomized controlled clinical trial[J]. Clinical Oral Implants Research, 2014, 25(2): e114-e119.

[8] Dar H Y, Azam Z, Anupam R, et al. Osteoimmunology: the nexus between bone and immune system[J]. Frontiers in Bioscience (Landmark Edition), 2018, 23: 464-492.

[9] 赵梓贺, 万熠, 于明志, 等. 激光刻蚀和阳极氧化对纯钛植入体表面性能的影响[J]. 中国表面工程, 2020, 33(6): 29-36.
Zhao Z H, Wan Y, Yu M Z, et al. Effects of laser etching and anodic oxidation on surface properties of pure titanium implants[J]. China Surface Engineering, 2020, 33(6): 29-36.

[10] Wang J J, Meng F H, Song W, et al. Nanostructured titanium regulates osseointegration via influencing macrophage polarization in the osteogenic environment[J]. International Journal of Nanomedicine, 2018, 13: 4029-4043.

[11] Zwahr C, Welle A, Weingärtner T, et al. Ultrashort pulsed laser surface patterning of titanium to improve osseointegration of dental implants[J]. Advanced Engineering Materials, 2019, 21(12): 1900639.

[12] Afanasiev Y V, Chichkov B N, Demchenko N N, et al. Ablation of metals by ultrashort laser pulses: theoretical modeling and computer simulations[J]. Journal of Russian Laser Research, 1999, 20(2): 89-115.

[13] Tang J P, Zhang Y C, Yao Y S, et al. High-performance ultrafine bubble aeration on janus aluminum foil prepared by laser microfabrication[J].

Langmuir: the ACS Journal of Surfaces and Colloids, 2021, 37(23): 6947-6952.

[14] Yong J L, Bai X, Yang Q, et al. Filtration and removal of liquid polymers from water (polymer/water separation) by use of the underwater superpolymphobic mesh produced with a femtosecond laser[J]. Journal of Colloid and Interface Science, 2021, 582(B): 1203-1212.

[15] Zuo P, Jiang L, Li X, et al. Phase-reversed MoS$_2$ nanosheets prepared through femtosecond laser exfoliation and chemical doping[J]. The Journal of Physical Chemistry C, 2021, 125(15): 8304-8313.

[16] Li X L, Xu J, Zhang A D, et al. Laser multifunctional fabrication of metallic microthermal components embedded in fused silica for microfluidic applications[J]. Optics & Laser Technology, 2021, 144: 107413.

[17] Lin Z J, Xu J, Song Y P, et al. Freeform microfluidic networks encapsulated in laser-printed 3D macroscale glass objects[J]. Advanced Materials Technologies, 2020, 5(2): 1900989.

[18] Wu D, Qi X B, Cai Z, et al. Direct generation of Airy beams at designed Fourier planes using integrated airy phase plates[J]. IEEE Photonics Technology Letters, 2021, 33(12): 595-598.

[19] Wang F F, Jiang L, Sun J Y, et al. One-step fabrication method of GaN films for internal quantum efficiency enhancement and their ultrafast mechanism investigation[J]. ACS Applied Materials & Interfaces, 2021, 13(6): 7688-7697.

[20] Yong J L, Zhuang J, Bai X, et al. Water/gas separation based on the selective bubble-passage effect of underwater superaerophobic and superaerophilic meshes processed by a femtosecond laser[J]. Nanoscale, 2021, 13(23): 10414-10424.

[21] 张玉梅, 赵铱民, 黄平, 等. 钛表面处理后表面能分析及对细胞附着的影响[J]. 稀有金属材料与工程, 2004, 33(5): 518-521.
Zhang Y M, Zhao Y M, Huang P, et al. Surface energy analysis of treated titanium and effects on cell adhesion[J]. Rare Metal Materials and Engineering, 2004, 33(5): 518-521.

[22] Chen P, Aso T, Sasaki R, et al. Adhesion and differentiation behaviors of mesenchymal stem cells on titanium with micrometer and nanometer-scale grid patterns produced by femtosecond laser irradiation[J]. Journal of Biomedical Materials Research A, 2018, 106(10): 2735-2743.

[23] Yang L, Ji S Y, Xie K N, et al. High efficiency fabrication of complex microtube arrays by scanning focused femtosecond laser Bessel beam for trapping/

releasing biological cells[J]. Optics Express, 2017, 25(7): 8144-8157.

[24] Yong J L, Huo J L, Yang Q, et al. Femtosecond laser direct writing of porous network microstructures for fabricating super-slippery surfaces with excellent liquid repellence and anti-cell proliferation[J]. Advanced Materials Interfaces, 2018, 5(7): 1701479.

[25] Chu D K, Yao P, Huang C Z. Anti-reflection silicon with self-cleaning processed by femtosecond laser[J]. Optics & Laser Technology, 2021, 136: 106790.

[26] 孟雪. 飞秒激光烧蚀固体材料的过程及表面形貌研究[D]. 济南: 山东师范大学, 2015: 30-32.
Meng X. The study of femtosecond laser ablation process and surface morphology of solid materials[D]. Jinan: Shandong Normal University, 2015: 30-32.

[27] Mannion P T, Magee J, Coyne E, et al. The effect of damage accumulation behaviour on ablation thresholds and damage morphology in ultrafast laser micro-machining of common metals in air[J]. Applied Surface Science, 2004, 233(1/2/3/4): 275-287.

[28] Bieda M, Lasagni A F, Beyer E. Fabrication of hierarchical microstructures on metals by means of direct laser interference patterning[J]. ICALEO, 2010: 900-907.

[29] Ahmmed K M T, Grambow C, Kietzig A M. Fabrication of micro/nano structures on metals by femtosecond laser micromachining[J]. Micromachines, 2014, 5(4): 1219-1253.

[30] 刘树青, 胡洁, 赵梦娇. 飞秒激光诱导周期性表面结构及其应用[J]. 科学通报, 2016, 61(14): 1560-1573.
Liu S Q, Hu J, Zhao M J. Femtosecond laser-induced periodic surface structure and its applications[J]. Chinese Science Bulletin, 2016, 61(14): 1560-1573.

[31] Du G Q, Yang Q, Chen F, et al. Dynamic near-field nanofocusing by V-shaped metal groove via a femtosecond laser excitation[J]. Applied Physics A, 2016, 122(3): 185.

[32] Bizi-Bandoki P, Benayoun S, Valette S, et al. Modifications of roughness and wettability properties of metals induced by femtosecond laser treatment[J]. Applied Surface Science, 2011, 257(12): 5213-5218.

[33] Dalawai S P, Aly M A S, Latthe S S, et al. Recent advances in durability of superhydrophobic self-cleaning technology: a critical review[J]. Progress in Organic Coatings, 2020, 138: 105381.

[34] Yong J L, Yang Q, Guo C L, et al. A review of femtosecond laser-structured superhydrophobic or

underwater superoleophobic porous surfaces/materials for efficient oil/water separation[J]. RSC Advances, 2019, 9(22): 12470-12495.

[35] 潘瑞, 张红军, 钟敏霖. 三级微纳超疏水表面的超快激光复合制备及防除冰性能研究[J]. 中国激光, 2021, 48(2): 0202009.
Pan R, Zhang H J, Zhong M L. Ultrafast laser hybrid fabrication and ice-resistance performance of a triple-scale micro/nano superhydrophobic surface[J]. Chinese Journal of Lasers, 2021, 48(2): 0202009.

[36] 江国琛, 潘瑞, 陈昶昊, 等. 超快激光制备水面减阻微纳结构及其耐蚀性研究[J]. 中国激光, 2020, 47(8): 0802005.
Jiang G C, Pan R, Chen C H, et al. Ultrafast laser fabricated drag reduction micro-nano structures and their corrosion resistance[J]. Chinese Journal of Lasers, 2020, 47(8): 0802005.

[37] Smeets R, Stadlinger B, Schwarz F, et al. Impact of dental implant surface modifications on osseointegration[J]. BioMed Research International, 2016, 2016: 6285620.

[38] 姜久仰, 刘宏宇, 张鹏, 等. 医用 Ti-6Al-4V 合金表面氟硅烷超疏水涂层的制备及生物学性能[J]. 稀有金属材料与工程, 2019, 48(6): 1884-1891.
Jiang J Y, Liu H Y, Zhang P, et al. Preparation and biological properties of the fluoroalkyl silane superhydrophobic coatings on biomedical Ti-6Al-4V alloy[J]. Rare Metal Materials and Engineering, 2019, 48(6): 1884-1891.

[39] Emelyanenko A M, Pytskii I S, Kaminsky V V, et al. Superhydrophobic copper in biological liquids: antibacterial activity and microbiologically induced or inhibited corrosion[J]. Colloids and Surfaces B, 2020, 185: 110622.

[40] Zeng Q Y, Zheng C Y, Han K, et al. A biomimic superhydrophobic and anti-blood adhesion coating[J]. Progress in Organic Coatings, 2020, 140: 105498.

[41] Long J Y, Zhong M L, Zhang H J, et al. Superhydrophilicity to superhydrophobicity transition of picosecond laser microstructured aluminum in ambient air[J]. Journal of Colloid and Interface Science, 2015, 441: 1-9.

[42] Wenzel R N. Resistance of solid surfaces to wetting by water[J]. Industrial & Engineering Chemistry, 1936, 28(8): 988-994.

[43] Long J Y, Zhong M L, Fan P X, et al. Wettability conversion of ultrafast laser structured copper surface[J]. Journal of Laser Applications, 2015, 27(S2): S29107.

[44] Child T F, van Ooij W J. Application of silane technology to prevent corrosion of metals and improve paint adhesion[J]. Transactions of the IMF, 1999, 77(2): 64-70.

[45] 罗晓, 刘伟建, 张红军, 等. 超快激光制备金属表面可控微纳二级结构及其功能化[J]. 中国激光, 2021, 48(15): 1502002.
Luo X, Liu W J, Zhang H J, et al. Ultrafast laser fabricating of controllable micro-nano dual-scale metallic surface structures and their functionalization[J]. Chinese Journal of Lasers, 2021, 48(15): 1502002.

[46] 江雷. 从自然到仿生的超疏水纳米界面材料[J]. 化工进展, 2003, 22(12): 1258-1264.
Jiang L. Nanostructured materials with superhydrophobic surface: from nature to biomimesis[J]. Chemical Industry and Engineering Progress, 2003, 22(12): 1258-1264.

[47] Cassie A B D, Baxter S. Wettability of porous surfaces[J]. Transactions of the Faraday Society, 1944, 40: 546-551.

[48] Chodniewicz D, Klemke R L. Guiding cell migration through directed extension and stabilization of pseudopodia[J]. Experimental Cell Research, 2004, 301(1): 31-37.

Fabrication and Cell-Adhesion Evaluation of Laser-Ablated Microprotrusion or Microgroove on Titanium

He Wanying[1,2], Yao Peng[1,2*], Chu Dongkai[1,2], Sun Huiqiang[3], Lai Qingguo[4],

Wang Qingwei[1,2], Wang Pengfei[1,2], Qu Shuoshuo[1,2], Huang Chuanzhen[5]

[1] *Center for Advanced Jet Engineering Technologies (CaJET)*, *School of Mechanical Engineering*,
Shandong University, *Jinan* 250061, *Shandong*, *China*;

[2] *Key Laboratory of High Efficiency and Clean Mechanical Manufacture*, *Shandong University*,
Ministry of Education, *Jinan* 250061, *Shandong*, *China*;

[3] *Department of Prosthodontics*, *School of Stomatology*, *Shandong University*, *Jinan* 250012, *Shandong*, *China*;

[4] *Department of Oral and Maxillofacial Surgery*, *the Second Hospital of Shandong University*,
Jinan 250033, *Shandong*, *China*;

[5] *School of Mechanical Engineering*, *Yanshan University*, *Qinhuangdao* 066004, *Hebei*, *China*

Abstract

Objective Titanium is widely used as an implant material owing to its excellent mechanical properties and good biocompatibility. It is often used in the manufacturing of artificial joints, bone plates, dental implants, etc. To improve the stability, antibacterial resistance, and abrasion resistance of titanium implants in organisms, their surface must be modified. An ultrafast laser can actively control the surface processing area and afford oxide layers, promoting cell adhesion. Currently, some researchers have realized many functions of titanium. However, the processes of such functions are complex and fewer types of structures are realized. Therefore, this study investigates the direct writing of microprotrusion and microgroove on titanium by modifying the processing parameters of femtosecond and picosecond lasers, systematically analyzes the difference in the microtexture, and explores a post-treatment method for regulating wettability. Finally, cell adhesion and proliferation experiments are performed to evaluate the biological properties of different microtextured surfaces.

Methods Titanium samples with a size of 10 mm were mechanically ground and polished. The samples were cleaned two times using ethanol for 10 min each time and then dried in air. Herein, both femtosecond laser (Spectra Physics Spitfire Ace; pulse width: 35 fs, wavelength: 800 nm, and repetition frequency: 1 kHz) and picosecond laser (BGL-1064-50B; pulse width: 15 ps, wavelength: 1064 nm, and repetition frequency: 10−1000 kHz) were used to ablate the titanium surface. For a comparison of hydrophilicity stability, the samples were separately stored in air, vacuum, and a 0.9% NaCl solution. The modified samples were immersed in a 1% fluoroalkylsilane solution (in ethanol) for one day to reduce the surface energy and then dried naturally. The ablated samples were loaded with rat bone marrow mesenchymal stem cells (rBMSCs) in a 24-well plate and cultured for 48 h. After immersing the cells with a 4% paraformaldehyde solution, dehydrating the cells with ethanol, and drying naturally, the samples were sprayed with gold to observe their morphology. The loaded samples were cultured for one, three, and five days and then mixed with a CCK-8 solution to measure their absorbance. The surface morphology and elemental content of the samples were characterized using scanning electron microscopy (JSM-6610LV) and energy dispersive spectroscopy (EDS). The surface profiles of the samples were observed using a VK-X200 confocal laser microscope. The surface wettability was evaluated using a contact angle measurement device (SDC-200S). The absorbance at 450 nm was measured using a M200 PRO NanoQuant microplate reader.

Results and Discussions Herein, both femtosecond and picosecond lasers were used to prepare microprotrusions and microgrooves on titanium surfaces. When the spot diameter of the femtosecond laser increased and the laser influence decreased, the microgroove width gradually increased while the depth decreased and both the width and height of the microprotrusion increased. As the overlapping rate decreased, the microgroove approached a U shape and the top of the microprotrusion became sharp (Fig. 3). The size of the microprotrusion ablated by the picosecond laser was considerably larger than that of the microgroove. When the laser influence or overlapping rate increased, the width and height of the microprotrusion increased. The EDS results revealed that the oxygen content in the picosecond laser-ablated surface was higher than that in the femtosecond laser-ablated surface (Fig. 5). After

modifying using the femtosecond and picosecond lasers, the contact angle of the titanium surfaces reduced from 40.25° to 9.88° and 0°, respectively. When the samples were stored in vacuum and the 0.9% NaCl solution, the picosecond laser-ablated arrays could maintain good superhydrophilicity. The silanization could reduce the surface energy of the sample without laser modification, femtosecond laser-ablated sample, and picosecond laser-ablated sample, yielding contact angles of 113.63°, 152.80°, and 146.38°, respectively (Fig. 6). The cells were mostly adhered along the top and edge strips of the microprotrusion and inside the microgroove processed using the femtosecond laser (Fig. 7). The cell proliferation results were consistent with the cell adhesion results (Fig. 8). Although the number of cells adhering to the picosecond laser-ablated surface was relatively small to the femtosecond laser-ablated surface, the picosecond laser-ablated surface could still afford more pseudopodia and then improved the cells spread on the top of the microprotrusion and the edge of the microgroove (Fig. 9).

Conclusions Herein, femtosecond and picosecond lasers were used to prepare a conventional microgroove and a special microprotrusion structure on titanium. The size of the structures ablated using both the lasers was mainly affected by the laser influence, while their shape was influenced by the overlapping rate. The oxygen contents in the femtosecond laser- and picosecond laser-ablated surfaces could reach 20.22% and 38.32%, respectively. Because the surface wettability was mainly affected by different microtexture morphologies, the contact angle of the titanium surface after femtosecond laser ablation decreased from the 40.25° to 9.88°, while that of the picosecond laser-ablated surface reached 0°. When the samples were stored in vacuum or a 0.9% NaCl solution for three days, the picosecond laser-ablated surface could maintain stable superhydrophilicity. Combined with silanization, the femtosecond laser-ablated surface became superhydrophobic at a contact angle of 152.80°, while the contact angle of the picosecond laser-ablated surface was 146.38°. Furthermore, the microprotrusion or microgroove arrays processed using the femtosecond laser were conducive to cell adhesion and arrangement, while those prepared using the picosecond laser promoted the growth of the pseudopodia of cells, thereby facilitating cell spreading and migration. The cell proliferation results were consistent with the cell adhesion results, showing that femtosecond laser processing could likely promote osteogenic differentiation. The combination of ultrafast laser-based micro/nano processing and hydrophilic/hydrophobic surface preparation technology can enhance the surface activity of titanium implants.

Key words laser technique; titanium; microprotrusion; microgroove; wettability; biocompatibility